Published in final edited form as:
Magn Reson Med. 2010 June ; 63(6): 1520–1528. doi:10.1002/mrm.22373.

Accelerating Time-Resolved MRA With Multiecho Acquisition

Hyun J. Jeong[1,*], **Christopher S. Eddleman**[2], **Saurabh Shah**[3], **Nicole Seiberlich**[4], **Mark A. Griswold**[4], **H. Hunt Batjer**[2], **James C. Carr**[5], and **Timothy J. Carroll**[1,5]

[1]Biomedical Engineering, Northwestern University, Chicago, Illinois, USA.

[2]Neurosurgery, Northwestern University, Chicago, Illinois, USA.

[3]Siemens Medical Solutions, Chicago, Illinois, USA.

[4]Radiology, University Hospitals of Cleveland, Cleveland, Ohio, USA.

[5]Radiology, Northwestern University, Chicago, Illinois, USA.

Abstract

A new four-dimensional magnetic resonance angiograpy (MRA) technique called contrast-enhanced angiography with multiecho and radial *k*-space is introduced, which accelerates the acquisition using multiecho while maintaining a high spatial resolution and increasing the signal-to-noise ratio. An acceleration factor of approximately 2 is achieved without parallel imaging or undersampling by multiecho (i.e., echo-planar imaging) acquisition. SNR is gained from (1) longer pulse repetition times, which allow more time for T_1 regrowth; (2) decreased specific absorption rate, which allows use of flip angles that maximize contrast at high field; and (3) minimized effects of a transient contrast bolus signal with a shorter temporal footprint. Simulations, phantom studies, and in vivo scans were performed. Contrast-enhanced angiography with multiecho and radial *k*-space can be combined with parallel imaging techniques such as Generalized Autocalibrating Partially Parallel Acquisitions to provide additional 2-fold acceleration in addition to higher SNR to trade off for parallel imaging. This technique can be useful in diagnosing vascular lesions where accurate dynamic information is necessary.

Keywords

multiecho; radial; MRA; time-resolved; 4D; contrast-enhanced; CAMERA

Although contrast-enhanced MRA (CE-MRA) is performed routinely in many clinical applications, X-ray digital subtraction angiography remains the current clinical standard for fast time-resolved angiography of the intracranial vasculature due to its superior spatial and temporal resolution. Despite the disadvantages of X-ray angiography, which involves catheterization, ionizing radiation, and nephrotoxic contrast agents, it offers high temporal and spatial resolutions required to image neurovascular conditions, often with abnormally high blood velocity.

In order to successfully image the hemodynamics of vascular lesions, the arterial phase of blood transit ideally is imaged without venous enhancement; for diseases such as arteriovenous malformations (AVMs), a temporal resolution even higher than what is required for artery-vein separation is necessary to image the filling and the draining patterns. Time-resolved MRA

*corresponding author to: Timothy J. Carroll, PhD, t-carroll@northwestern.edu. 737 N. Michigan Ave., Suite 1600, Chicago, IL 60611.

is generally performed by repeating the acquisition of full *k*-space data during the first pass of contrast agent in order to obtain multiple frames capturing the movement of the contrast bolus (in this work, each repeated *k*-space data set will be called "measurements"). However, the acquisition times for a fully sampled set of MR data tend to be lengthy, lasting about 10 sec or more for one measurement without parallel imaging, depending on the desired spatial resolution. This makes time-resolved imaging difficult if subsecond temporal resolution is desired.

There have been many successful attempts to perform first-pass contrast-enhanced time-resolved MRA (1–10), yet there is still a demand for higher spatial and temporal resolution while maintaining sufficient SNR. However, in order to increase the SNR, spatial resolution, or temporal resolution, the other two desired properties must generally decrease in a standard MRI scan.

Despite many improvements in time-resolved CE-MRA, there are currently no techniques with diagnostic confidence to replace the X-ray digital subtraction angiography as a primary imaging modality for AVMs. In order to obtain temporal information faster than the acquisition rate of a full data set, previously developed techniques either undersample parts of *k*-space (2–4) or extract temporal information from the data collected over a relatively long period of time (1,7,8). However, many investigators now agree that even though some techniques achieve a higher rate of image update, the temporal resolution ultimately depends on the "temporal footprint" (9) (also known as "temporal window" or "temporal aperture"), which is the span of the time window in which all the *k*-space points used to reconstruct a single image are acquired. Therefore, the only way to truly increase the temporal resolution is to decrease the acquisition time of a single frame.

In this paper, a new four-dimensional MRA technique called contrast-enhanced angiography with multi-echo and radial *k*-space (CAMERA) is introduced, which accelerates the acquisition using multiple echoes while maintaining sufficient spatial resolution. Acceleration factors of approximately 2 are achieved using an echo train length of 4 without parallel imaging or undersampling. Because of T_2^* shortening with gadolinium (Gd) and signal decay from the long pulse repetition time (TRs) associated with multiecho acquisitions, one would expect a signal loss; however, signal is intrinsically recovered in three ways. First, the acceleration in the acquisition increases SNR in MRA when the contrast agent signal is transient (11,12). Second, increase in TR from multiecho imaging allows more time for regrowth of longitudinal magnetization. Last, the longer TR decreases the specific absorption rate (SAR), allowing the sequence to run at the flip angle that maximizes Gd-background contrast. For high-field magnets (3 T or higher), SAR is a limiting factor for fast sequences like spoiled gradient echo used for time-resolved MRA, which requires the MRA sequence to be performed with a longer TR or a lower flip angle (13). The purpose of this work is to compare CAMERA with the previously developed single-echo technique (8) and to a parallel-imaging technique that provides approximately the same acceleration as CAMERA. Furthermore, the feasibility of combining CAMERA with parallel imaging is explored.

MATERIALS AND METHODS

Sequence Description

In CAMERA, data are acquired in radially sampled in-plane and Cartesian through-plane *k*-space, or "stack of stars." Multiple echoes are used in the partition direction in an interleaved manner to cover multiple partitions during each TR, similar to segmented echo-planar imaging (14–16). The multiecho partitions are acquired in a centric reordering scheme, which ensures that the central *k*-space region always contains the first readouts of the echo trains, as well as the same readout polarity. This method has been shown to reduce flow-related artifacts in echo-

planar imaging (17,18). Acquiring the central *k*-space during the first echo is particularly important for CE-MRA because T_2^* shortening from Gd contrast agent may cause signal loss as the echo time (TE) becomes longer. The radial views are ordered in a pseudorandom scheme, in which the angles are not acquired in linearly increasing order from 0° but in a predefined order described in Cashen et al. (8). A partial echo has been used for each readout, which omitted F1 sampling of the first 25% of the readout. Figure 1 illustrates the sampling schemes of CAMERA. In the remainder of this manuscript, a naming convention will be used where the integer following E (number of echoes) corresponds to the echo train length. Then, a CAMERA with echo train length of 1 (E1) is identical to radial three-dimensional spoiled gradient echo without multiecho. Sliding-window reconstruction was applied to further increase the frame rate (1,8). In addition, GRAPPA (19) can be combined with CAMERA by skipping interleaves. The autocalibration lines are obtained prior to contrast injection by acquiring a full set of data without skipping any lines.

Simulations

In order to estimate how much acceleration will be gained using CAMERA, acquisition times were calculated using durations of the radiofrequency pulses and gradients from a typical protocol for each echo train length: N_{RO} (readout points per projection) = 192, N_{proj} (number of radial projections) = 192, $N_{Partition}$ (number of three-dimensional slices) = 32, field of view = 220 × 220 × 96 mm. The acquisition times were divided by the duration for E1 to obtain relative acquisition times.

In order to visualize the effects of reduced temporal footprint, an injected bolus was simulated with a rectangular bolus, with a size of 4 × 4 × 20 mm^3, moving at 5 mm/sec. The bolus was modeled as a combination of sinc functions varying in time and spatial frequency because they can be analytically transformed between image domain and *k*-space, as described elsewhere (8,20). The model is then sampled first with simulated three-dimensional radial stack-of-stars acquisition. The sampling is repeated with half the acquisition time to show the effect of a temporal footprint on a moving object.

Static Phantoms

SNR was quantified by imaging four plastic vials, each containing 40 mL of 0.5-mol/L Gd diethylenetriamine penta-acetic acid (Gd-DTPA) (Magnevist; Berlex, Wayne, NJ) solution diluted to 1%, 2%, 4%, and 6.5% Magnevist by volume, which was assumed to be close to in vivo concentrations in a typical protocol. The vials were submerged in tap water, placed in a Siemens 3T Trio scanner (Siemens AG, Erlangen, Germany), and imaged with a Siemens phased-array body matrix and spine array, for a total of 12 channels. A weight of 150 lbs was entered to the system for realistic SAR calculation. The phantoms were scanned in the coronal plane with the CAMERA sequence, with echo train lengths of 1, 4, and 8. The phantoms were also imaged with 2× GRAPPA in the slice direction with E1 and E4 for comparison between two techniques with approximately the same temporal footprint and to explore the possibility of combining GRAPPA and this multiecho acquisition schemes. Table 1 summarizes the imaging parameters for each protocol. In a separate scan, vials filled with 1%, 2%, and 4% dilutions of contrast were imaged with E1, E2, E4, E8, and E16 to observe the effects of increasing echo train lengths on image quality in the coronal plane. The following image parameters were used: N_{RO} = 192 (after zero-filling for partial echo), N_{proj} = 192, $N_{partition}$ = 32, and field of view = 220 × 220 × 96 mm, resulting in a resolution of 1.1 × 1.1 × 3 mm. Minimum achievable TR/TE values were used, which depended on the echo train length. For E4, a TR of 6.2 ms and TEs of 1.4, 2.4, 3.4, and 4.4 ms were used. The flip angle was varied from 5° to 55° (or until the SAR limit was reached) in 5° increments to find the flip angles that result in highest contrast-to-noise ratio (CNR) between Gd and background for each echo train length. Regions of interest were drawn on the phantoms in the central slice to calculate SNR.

Flow Phantom

In order to verify the SNR and temporal fidelity in a controlled setting, a 3-inch piece of silicone tubing (inner diameter ~3/8 inch) was imaged while diluted contrast agent was flowing through it. The tube was submerged in a waterbath and connected to a power injector (Spectris Solaris; Medrad, Indianola, PA) containing 2% Magnevist diluted with saline. Ten milliliters of diluted contrast agent was injected at 4 mL/sec, followed by the same rate and volume of saline flush. As with the static phantoms, a Siemens 3T Trio scanner (Siemens AG) was used with a Siemens phased-array body matrix and spine array, for a total of 12 channels. Imaging parameters were the same as those of the static phantom scans, but multiple measurements were imaged with sliding-window reconstruction for dynamic imaging. The flip angles used were 25° for E1 and 35° for E4, which were determined to be optimal in the phantom studies. The first frame was subtracted from all images to remove background signal. A total of 16 intermediate frames between measurements were reconstructed for each data set, using the sliding-window reconstruction. Circular regions of interest were drawn over the tube and background to measure SNR for each reconstructed frame.

In Vivo Study

A total of 15 healthy volunteers were scanned using the Siemens 3T Trio scanner with a Siemens 12-channel head coil. The studies were approved by the institutional review board. A total of five volunteers were scanned with E1, two volunteers were scanned with E1-GRAPPA, four volunteers were scanned with E4, and two volunteers were scanned with E4-GRAPPA. Subjects were scanned in the sagittal plane to cover one hemisphere of the brain, which is the clinical protocol used for AVM imaging at our site. Two volunteers were also scanned using the hybrid E4-GRAPPA in a sagittal plane that covered the whole head.

The imaging parameters for the hemisphere scans were identical to the flow phantom study. Imaging parameters for the whole-head MRA were the same, except for $N_{partition} = 48$ (3.2 mm slices), and a nonselective excitation pulse was used, which reduces the TR by approximately 0.8 ms to 5.5 ms for E4.

For all scans, a single dose (0.1 mmol/kg) of Magnevist was administered with a power injector at 4 mL/sec, followed by 20 mL of saline at 4 mL/sec, a protocol established in our previous MRA studies. Expected blood Gd concentration was calculated using the formula in Maki et al. (21). The flip angle that resulted in a maximum SNR from the phantoms at that Gd concentration was chosen. Sliding subtraction (8) was used for improved arterial-venous separation, with a subtraction interval of approximately 10 sec. Two AVM patients were each scanned with E4 and E4-GRAPPA, and the resulting images correlated with an X-ray angiogram of the same patient.

SNR Analysis

Noise distributions of images from raw MR data that have undergone regridding or GRAPPA processing tend to be inconsistent. Hence, the method of calculating SNR based on the average signal divided by the standard deviation of signal-free region may not be accurate for the reconstruction methods used in this study. To address this problem, SNRs for the static and flow phantoms were calculated using bootstrap statistics proposed by Riffe et al. (22). Noise data were acquired for the same imaging protocol, with no radiofrequency pulse. The noise was randomly redistributed for each channel, and the reconstruction was repeated 100 times. Voxel-by-voxel SNR values were obtained by dividing the mean intensity by the standard deviation of the same voxel. Each voxel was averaged to obtain an SNR value within a region of interest.

RESULTS

Simulations

Acceleration factors that can be achieved using multiecho acquisitions are shown in Fig. 2; as the echo train length increases, so does the possible acceleration as compared with the single-echo (E1) acquisition. For example, E4 allows an acceleration factor just over 2, while a 3-fold acceleration is possible with E16. An echo train length of 4 was mainly for this study to achieve 2× acceleration.

Figure 3 shows the effect of the temporal footprint when using data from different time points to reconstruct an image. With E4, which has about 50% of the temporal footprint of E1, the moving bolus closely represents the true image. The reconstruction using the E1 acquisition, however, depicts an elongated and spatially blurred contrast bolus. Thus, a reduction in the temporal footprint by even a factor of 2 greatly increases the temporal fidelity of the reconstructed image.

Static Phantoms

Figure 4 shows the plot of SNR values with varying flip angles for vials containing 1%, 2%, 4%, and 6.5% dilutions of Magnevist. For E1 and E4, the highest flip angles possible within the SAR limit were 35° and 65°, respectively. For E1, the maximum SNR values were at flip angles between 25° and 30° for 1% and 2% Magnevist. For E4, the maximum SNR values were at flip angles between 35° and 45° for the same concentrations. For the 4% and 6.5% dilutions, the SNR increased with higher flip angles until the SAR limit. At their optimal flip angles, the maximum SNR of E4 was higher than that of E1, while the E4 acquisition had a temporal footprint twice as short as the E1 acquisition. Images acquired using an echo train length greater than 4 provided no significant acceleration and resulted in significant artifacts related to multiecho imaging (Fig. 5), which resulted in highly distorted images. Images acquired with CAMERA and GRAPPA in the partition direction showed significant decrease in SNR (~75% decrease). However, E4-GRAPPA and E1-GRAPPA produced similar SNR values.

Flow Phantom

Figure 6 shows plots of SNR versus time in a representative region of interest of the flow phantom for E1, E4, E1-GRAPPA, and E4-GRAPPA. As predicted by the simulations and the static phantoms, E4 shows significantly greater SNR than E1, as well as a narrower bolus profile. The decreased bolus width is indicative of less temporal blurring due to the shorter temporal footprint of the acquisition. E1-GRAPPA has approximately 1/2 and 1/3 of the SNR of E1 for 1% and 2% Gd, respectively, but benefits from a shorter temporal footprint, shown by the narrow width of the bolus profile, which is very close to the width of the curve of E4. The E4-GRAPPA curve shows slightly better SNR than E1-GRAPPA and a significantly narrower temporal profile than E1-GRAPPA or any other curve.

In Vivo Results

Arterial- and venous-phase images were selected from the dynamic series from E1, E4, E1-GRAPPA, and E4-GRAPPA reconstructions, shown in Fig. 7. The arterial phase was defined as the latest frame without the enhancement of the sagittal sinus. From visual inspection, E4 without GRAPPA has the highest signal with least amount of artifact. Enlarged images of the anterior cerebral artery show that multiecho (E4) is better able to image the anterior carotid artery branches than the single echo (E1). The GRAPPA versions of E1 and E4 perform poorly compared to the non-GRAPPA versions and show artifactual enhancement of the background (Fig. 7, dotted arrows). In their venous phases, the E4 acquisitions show better delineation of

smaller cortical vessels than the E1 acquisitions both with and without GRAPPA. Figure 8 shows a comparison of CAMERA-E4 and X-ray digital subtraction angiography of an AVM patient. With CAMERA-E4, the early drainage from AVM to the sigmoid sinus before sagittal sinus enhancement can be clearly observed. Figure 9 shows a whole-head four-dimensional MRA obtained with E4-GRAPPA, clearly demonstrating separation between arterial and venous phases.

DISCUSSION

We have found that multiecho CE-MRA can reduce the temporal footprint without compromising SNR. The decreased footprint improves the dynamic fidelity and image quality. Combining GRAPPA with CAMERA results in further reduction in the temporal footprint, and higher SNR of CAMERA provides more signal to be traded off for higher acceleration factors. In regard to the echo train length, it was determined that E4, with an acceleration of approximately 2, resulted in a good tradeoff between speed and image quality. Further increasing the echo train length did not increase the acceleration significantly but produced stronger artifacts related to multiecho imaging.

For static phantoms, E4 showed significantly higher SNR than E1 at low concentrations of Gd (1% and 2% dilutions) at optimal flip angles. Since the signal was not transient and optimal flip angles were used, the SNR increase is attributed to the fact that the longer TR of the E4 acquisition allows more time for the recovery of longitudinal magnetization at steady state. The effect of the TR increase is small for background tissue with long T_1 (e.g., ~900 ms for gray matter) compared to blood with Gd, which increase the overall blood-tissue contrast. In addition, the contrast is increased with the use of a larger flip angle. The GRAPPA versions of E1 and E4 show similar trends, but with significantly lower overall SNR, which was well below the expected $1/\sqrt{2}$. After reanalysis, we found that there is very little sensitivity variation in the through-plane direction. This implies that the coil configuration was suboptimal for this particular study, and with optimized coils, the CAMERA-GRAPPA could be improved.

From the flow-phantom study, it is clear that a shorter temporal footprint provides a narrower bolus profile. This is an important metric for time-resolved MRA as it determines how clearly the different phases of the bolus passage are separated. The SNR levels were similar to those observed in 2% phantom studies, which was expected since 2% dilution of contrast agent was injected. It has been shown that a shorter temporal footprint results in an SNR increase in MRA because a larger extent of *k*-space can be sampled closer to the peak phase of the transient contrast bolus signal (11,12). However, this has not been observed in the flow phantom study, probably because the contrast flow rate through the tube is slower than the blood flow in vivo and slow enough that the bolus peak is sufficiently covered by the temporal footprint of E1. Similar results were obtained with volunteer studies. E1, which had the longest temporal footprint, showed inferior depiction of smaller vessels, even though it showed good overall SNR and depiction of larger vessels compared to E4 (for the same reasons that caused SNR boost in the flow phantom study). The GRAPPA versions provided an additional 2-fold decrease in the temporal footprint. However, the additional signal boost shown in Riederer et al. (12) was offset by the intrinsic signal decrease from the GRAPPA algorithm, which may again be attributed to coil geometry. Despite this drawback, the acceleration obtained by using GRAPPA results in an additional narrowing of the temporal profiles, which may be useful in resolving very fast transit times of AVMs.

In this work, E4 was used for flow phantom and in vivo scans, although further accelerations are possible with CAMERA using longer echo train lengths. The reason for this limitation on the acceleration is that significant susceptibility artifacts begin to appear with longer echo train lengths. This is due to two effects: first, the susceptibility artifact, caused by T_2^* decay, becomes

significant for readouts with longer TEs. Readouts with longer TEs also suffer more from susceptibility artifacts from metal clips and other devices. Secondly, interleaved echo-planar imaging with more echoes per shot produces greater variations in *k*-space, which results in stronger ghost artifacts in the slice-encoding direction. This effect is more pronounced in CAMERA than other in-plane multiecho techniques because in CAMERA, multiecho encoding is performed in the through-plane direction, with only about 30 partitions acquired.

GRAPPA with 2-fold acceleration was compared with E4 because they both offer approximately the same temporal footprint compared to E1. Even with ideal GRAPPA reconstruction, E4 results in higher SNR than the GRAPPA technique, with a similar temporal footprint since E4 has greater SNR than the non-GRAPPA E1 acquisition. This allows more room to trade off SNR for higher acceleration factors when CAMERA and parallel imaging are combined. Figure 6 shows that there is significant reduction in the profile width from E4 to E4-GRAPPA, which means that E4 may not be fast enough to accurately portray the bolus passage, and combining parallel imaging may be necessary. GRAPPA has shown excellent results in CE-MRA in Cartesian *k*-space in MRA (23,24), but the sliding-window reconstruction is not well suited for Cartesian sampling (8). Other parallel-imaging methods can be considered, such as radial GRAPPA (25), which undersamples the projection angles, has been shown to be promising, and should be explored in the future with CAMERA. SENSE has also shown good results in other MRA techniques (9,26–28). CAMERA and parallel imaging methods are not competing techniques but can be used to complement one another. Maximum acceleration that can be achieved by CAMERA is at 2× (3× results in significant artifacts). Therefore, further acceleration, if necessary, must be achieved by other means such as parallel imaging. Because it is robust and has no significant SNR loss compared to the nonaccelerated version, CAMERA adds an extra 2-fold acceleration with increased SNR, which can be utilized by any parallel-imaging technique to further accelerate the acquisition.

With techniques such as keyhole (2,3) and Time-Resolved Imaging of Contrast Kinetics (TRICKS) (4), the high-frequency components are never updated or updated less often. Therefore, high-frequency information such as smaller vessels or aneurysms may be misrepresented. Even with the acceleration from undersampling the high-frequency data, TRICKS has not been shown to be fast enough for some applications, such as intracranial AVMs (29). Also, keyhole and TRICKS reconstruct images using data acquired from different points in time and not always from a contiguous time block, resulting in “jumpy” image updates, rather than smooth dynamic angiograms. CAMERA addresses this problem with a consistent and contiguous temporal footprint, resulting in a smooth image update. Sliding-window reconstruction can be used with image update as often as one projection to increase frame rate, though temporal resolution is also limited by the temporal footprint.

A limitation of this technique is that due to the interleaved partition acquisition ordering, the number of partitions is limited to multiples of $2 \times N_{echoes}$ for complete partition coverage. Therefore, in order to properly localize the scan in partition direction, partition thickness should be adjusted after setting the number of partitions. Also, the TE values must be carefully chosen so that there is no signal cancellation from chemical shift.

CONCLUSION

A four-dimensional MRA technique, CAMERA, allows for the acquisition of data, with a narrower temporal footprint and higher SNR than standard stack-of-stars trajectories, with approximately 2-fold acceleration without parallel imaging. The technique utilizes multiple echoes for an echo-planar imaging type acquisition in the through-plane direction of a cylindrical *k*-space. SNR is gained from longer TRs, which allow more time for T_1 regrowth while minimizing the effects of a transient contrast bolus signal with a shorter temporal

footprint. The CAMERA technique, combined with GRAPPA or another parallel-imaging techniques, could potentially be useful in the diagnosis of vascular lesions where accurate dynamic information is necessary.

REFERENCES

1. Riederer SJ, Tasciyan T, Farzaneh F, Lee JN, Wright RC, Herfkens RJ. MR fluoroscopy: technical feasibility. Magn Reson Med 1988;8:1–15. [PubMed: 3173063]
2. van Vaals JJ, Brummer ME, Dixon WT, Tuithof HH, Engels H, Nelson RC, Gerety BM, Chezmar JL, den Boer JA. “Keyhole” method for accelerating imaging of contrast agent uptake. J Magn Reson Imaging 1993;3:671–675. [PubMed: 8347963]
3. Jones RA, Haraldseth O, Muller TB, Rinck PA, Oksendal AN. k-Space substitution: a novel dynamic imaging technique. Magn Reson Med 1993;29:830–834. [PubMed: 8350729]
4. Korosec FR, Frayne R, Grist TM, Mistretta CA. Time-resolved contrast-enhanced 3D MR angiography. Magn Reson Med 1996;36:345–351. [PubMed: 8875403]
5. Goldfarb JW, Prasad PV, Griswold MA, Edelman RR. Dynamic three-dimensional magnetic resonance abdominal angiography and perfusion: implementation and preliminary experience. J Magn Reson Imaging 2000;11:201–207. [PubMed: 10713955]
6. Finn JP, Baskaran V, Carr JC, McCarthy RM, Pereles FS, Kroeker R, Laub GA. Thorax: low-dose contrast-enhanced three-dimensional MR angiography with subsecond temporal resolution—initial results. Radiology 2002;224:896–904. [PubMed: 12202730]
7. Mistretta CA, Wieben O, Velikina J, Block W, Perry J, Wu Y, Johnson K. Highly constrained backprojection for time-resolved MRI. Magn Reson Med 2006;55:30–40. [PubMed: 16342275]
8. Cashen TA, Jeong H, Shah MK, Bhatt HM, Shin W, Carr JC, Walker MT, Batjer HH, Carroll TJ. 4D radial contrast-enhanced MR angiography with sliding subtraction. Magn Reson Med 2007;58:962–972. [PubMed: 17969099]
9. Haider CR, Hu HH, Campeau NG, Huston J 3rd, Riederer SJ. 3D high temporal and spatial resolution contrast-enhanced MR angiography of the whole brain. Magn Reson Med 2008;60:749–760. [PubMed: 18727101]
10. Du J. Contrast-enhanced MR angiography using time resolved interleaved projection sampling with three-dimensional Cartesian phase and slice encoding (TRIPPS). Magn Reson Med 2009;61:918–924. [PubMed: 19195019]
11. Maki JH, Prince MR, Londy FJ, Chenevert TL. The effects of time varying intravascular signal intensity and k-space acquisition order on three-dimensional MR angiography image quality. J Magn Reson Imaging 1996;6:642–651. [PubMed: 8835958]
12. Riederer SJ, Hu HH, Kruger DG, Haider CR, Campeau NG, Huston J 3rd. Intrinsic signal amplification in the application of 2D SENSE parallel imaging to 3D contrast-enhanced elliptical centric MRA and MRV. Magn Reson Med 2007;58:855–864. [PubMed: 17969124]
13. Cashen TA, Carr JC, Shin W, Walker MT, Futterer SF, Shaibani A, McCarthy RM, Carroll TJ. Intracranial time-resolved contrast-enhanced MR angiography at 3T. AJNR Am J Neuroradiol 2006;27:822–829. [PubMed: 16611772]
14. McKinnon GC. Ultrafast interleaved gradient-echo-planar imaging on a standard scanner. Magn Reson Med 1993;30:609–616. [PubMed: 8259061]
15. Mugler JP 3rd, Brookeman JR. Off-resonance image artifacts in interleaved-EPI and GRASE pulse sequences. Magn Reson Med 1996;36:306–313. [PubMed: 8843385]
16. Lu A, Grist TM, Block WF. Fat/water separation in single acquisition steady-state free precession using multiple echo radial trajectories. Magn Reson Med 2005;54:1051–1057. [PubMed: 16217786]
17. Luk Pat GT, Meyer CH, Pauly JM, Nishimura DG. Reducing flow artifacts in echo-planar imaging. Magn Reson Med 1997;37:436–447. [PubMed: 9055235]
18. Beck G, Li D, Haacke EM, Noll TG, Schad LR. Reducing oblique flow effects in interleaved EPI with a centric reordering technique. Magn Reson Med 2001;45:623–629. [PubMed: 11283990]
19. Griswold MA, Jakob PM, Heidemann RM, Nittka M, Jellus V, Wang J, Kiefer B, Haase A. Generalized autocalibrating partially parallel acquisitions (GRAPPA). Magn Reson Med 2002;47:1202–1210. [PubMed: 12111967]

20. Jeong HJ, Cashen TA, Hurley MC, Eddleman C, Getch C, Batjer HH, Carroll TJ. Radial sliding-window magnetic resonance angiography (MRA) with highly-constrained projection reconstruction (HYPR). Magn Reson Med 2009;61:1103–1113. [PubMed: 19230015]

21. Maki JH, Chenevert TL, Prince MR. Three-dimensional contrast-enhanced MR angiography. Top Magn Reson Imaging 1996;8:322–344. [PubMed: 9402676]

22. Riffe M, Blaimer M, Barkauskas K, Duerk J, Griswold M. SNR estimation in fast dynamic imaging using bootstrapped statistics. Proc Int Soc Magn Reson Med 2007;15:1879.

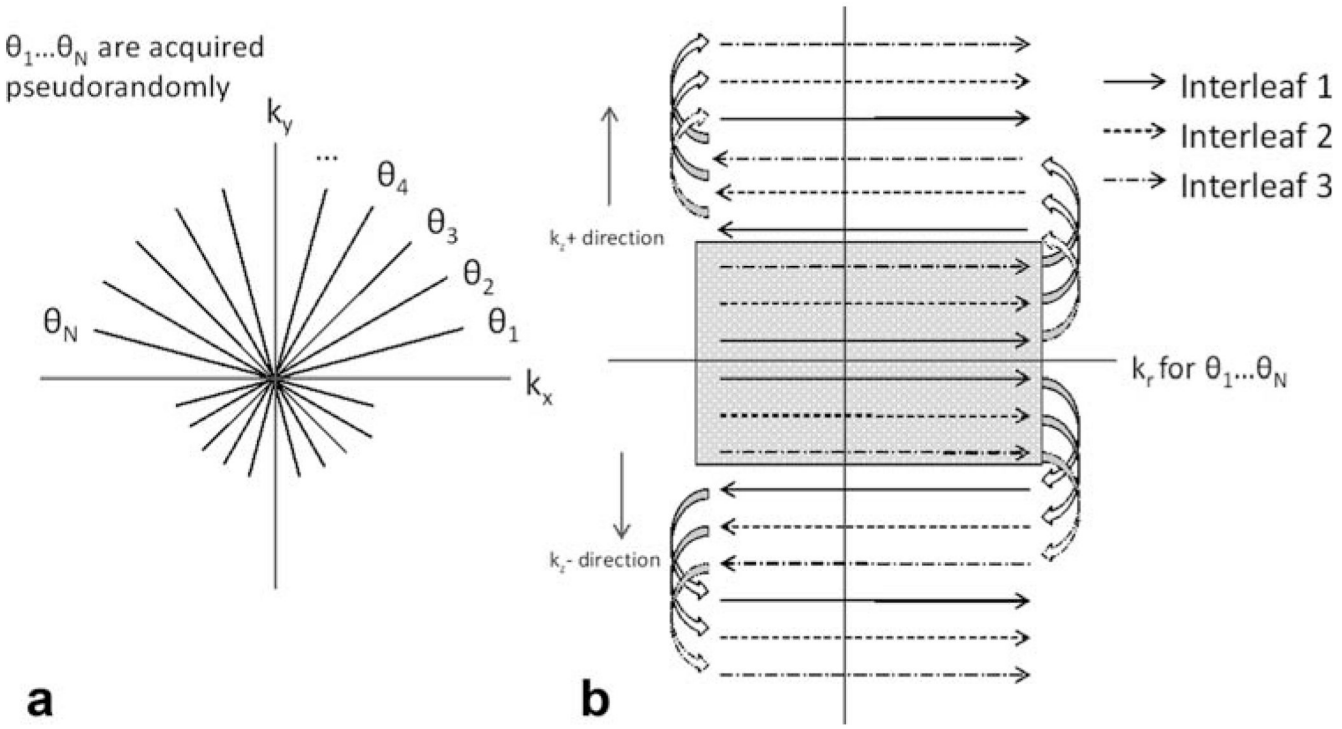

FIG. 1.

CAMERA acquisition. Data are acquired in three-dimensional radial "stack-of-stars" *k*-space. The innermost partition loop is acquired using a centric echo-planar imaging scheme. This ensures consistent readout polarity, as well as minimal T_2^* signal loss in the central region of the *kr*-*kz* plane.

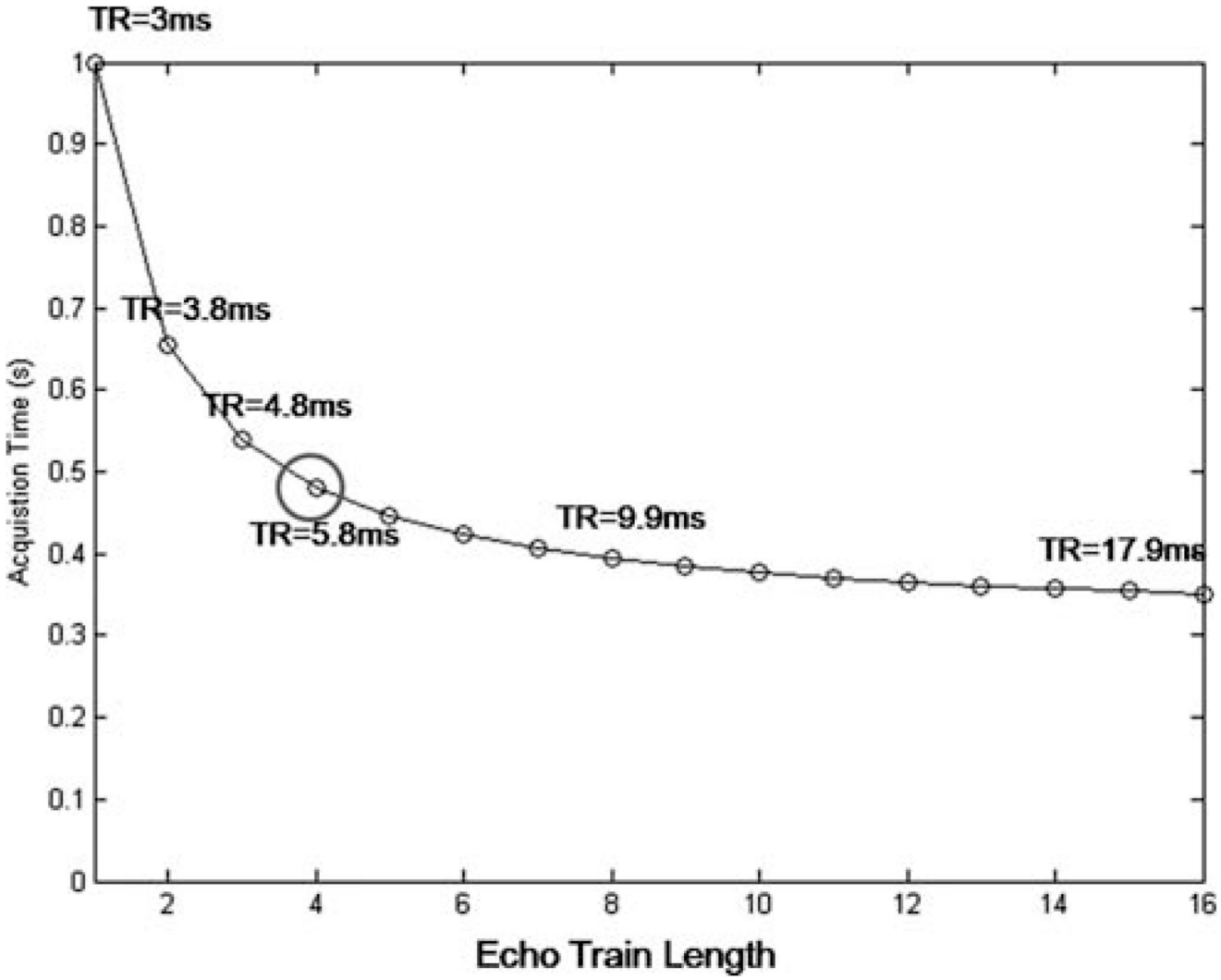

FIG. 2.

Reduction in acquisition time versus echo train length. An echo train length of 4 was used for this study. Although longer echo train lengths are possible, the gains in acceleration are not significant and introduce stronger artifacts related to multiecho imaging.

FIG. 3.

Simulations of the effects of the temporal footprint. The true image, a contrast bolus modeled by a simple box function, is blurred significantly with a slower temporal footprint of E1. With 50% reduction in the temporal footprint achieved by E4, the blur is decreased significantly.

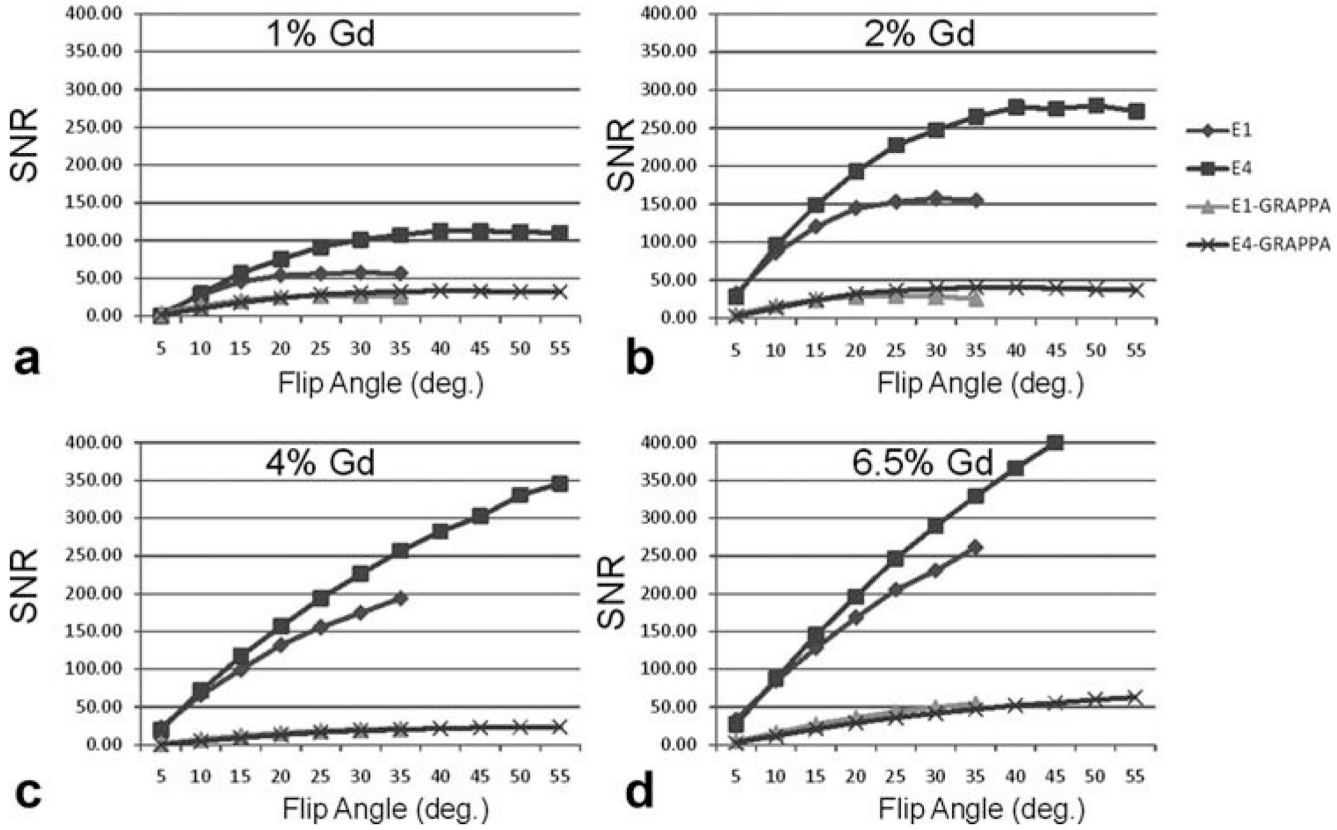

FIG. 4.

SNR versus flip angle. SNR values calculated using the bootstrap method have been plotted for varying flip angles. E4 has a significantly higher SNR than E1. GRAPPA versions of CAMERA show similar trends but lower SNR compared to non-GRAPPA reconstructions.

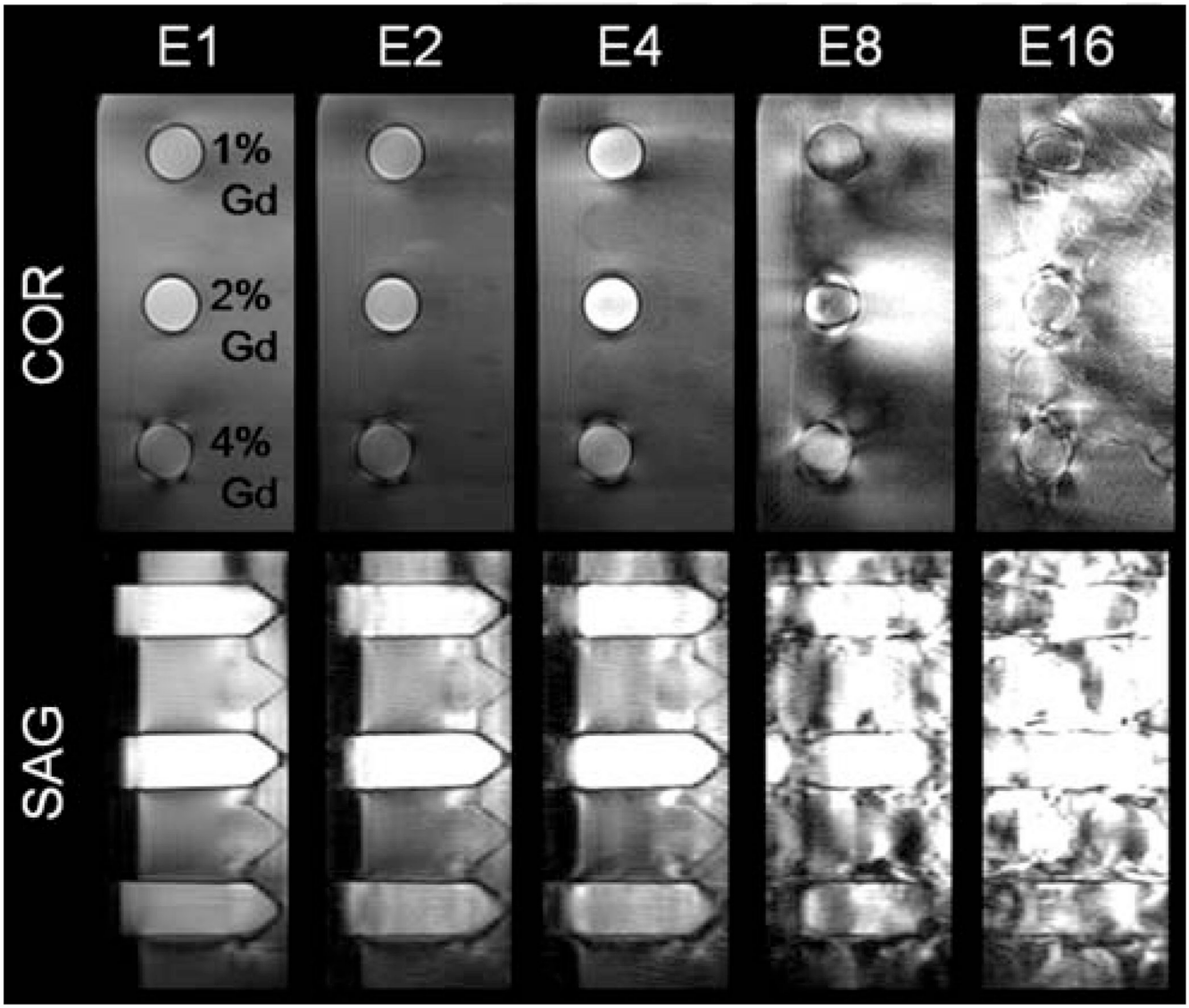

FIG. 5.
Degradation of image quality with increasing echo train length. Coronal (in-plane) and sagittal (through-plane) views of 1%, 2%, and 4% dilution of Magnevist (Berlex) were imaged with E1, E2, E4, E8, and E16. Echo train length greater than 4 results in images with severe artifacts.

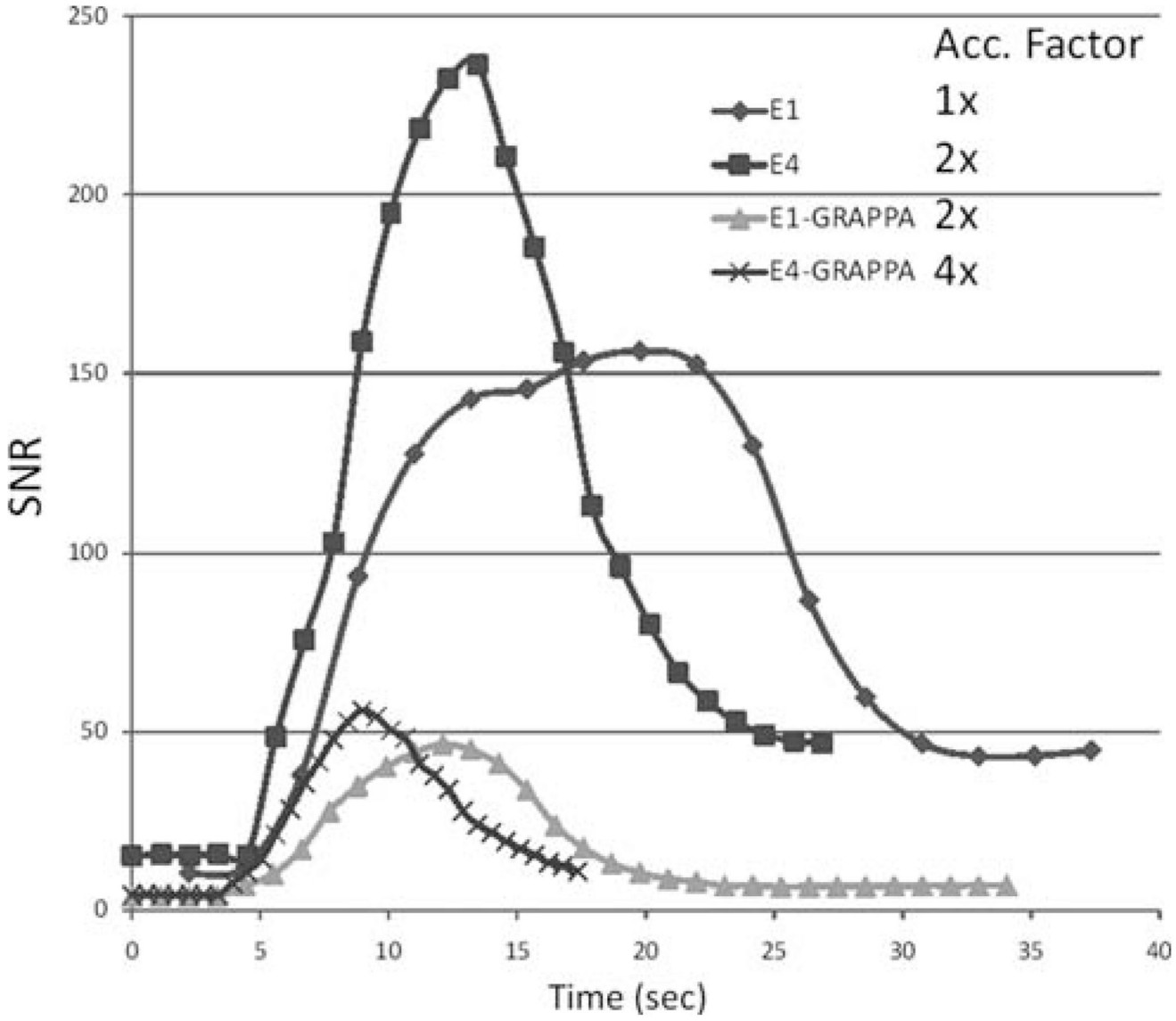

FIG. 6.

SNR of flow phantom versus time. SNR values calculated using the bootstrap method have been plotted over time. E4 has higher SNR and narrower temporal profile than E1 for both GRAPPA and non-GRAPPA versions. Overall, the temporal profile width is consistent with relative acceleration factors (indicated in the legend) of each technique compared to E1.

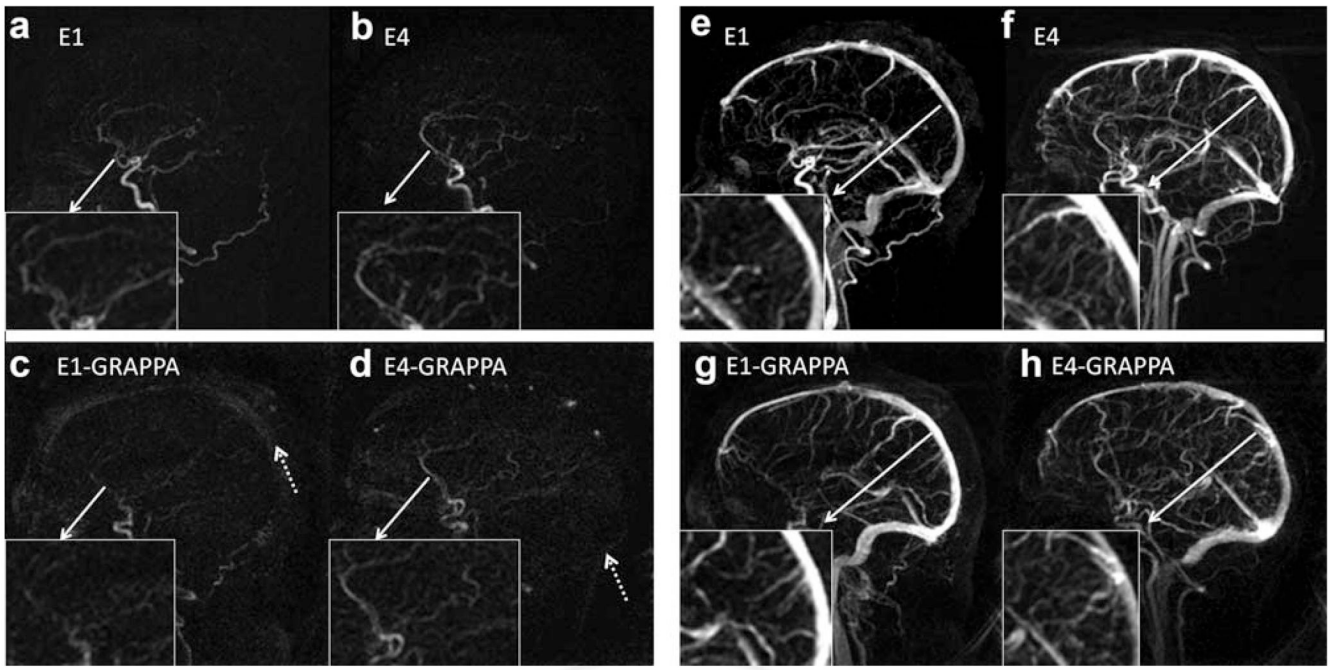

FIG. 7.

Arterial (left) and venous (right) phases of four-dimensional MRA using CAMERA of four volunteers. E4 shows superior image quality during the arterial phase, with better delineation of the ACA and E1, for both GRAPPA and non-GRAPPA versions. More smaller vessels are identified near the sagittal sinus during the venous phase with E4 than E1 acquisitions, both with and without GRAPPA.

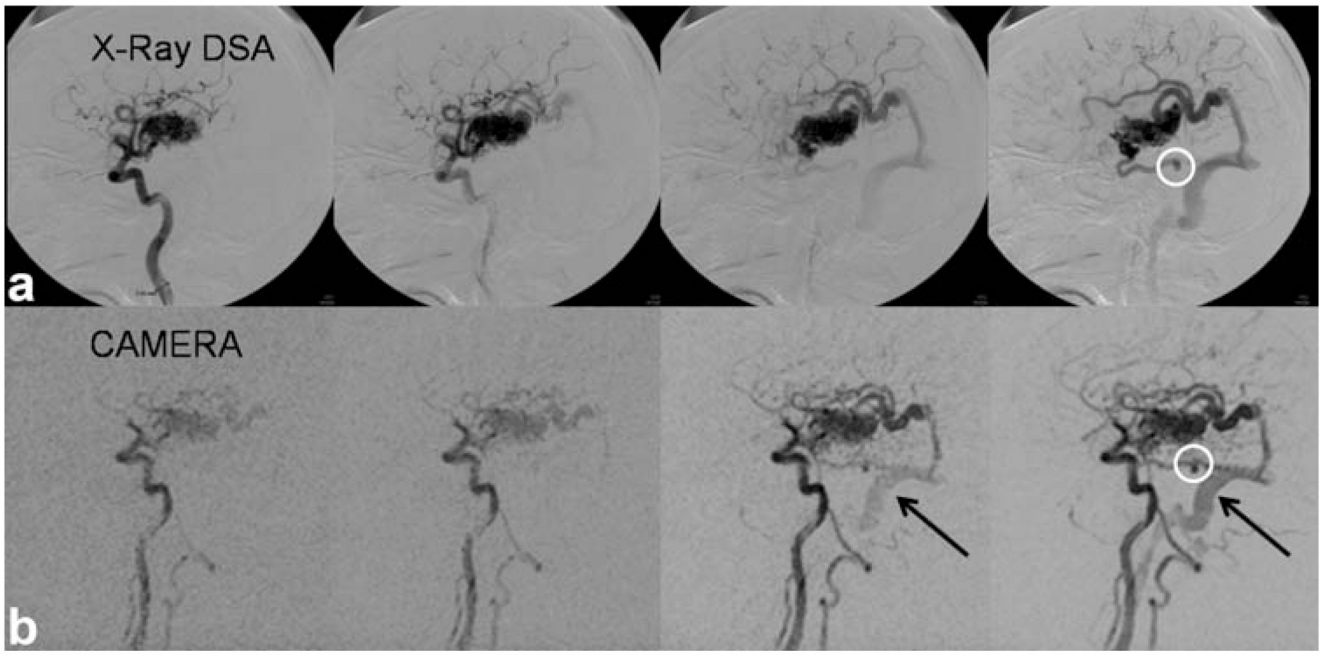

FIG. 8.

AVM patient image acquired with E4 (inverted). Comparison with X-ray digital subtraction angiography images show close correlation. Early drainage from the AVM to the sigmoid sinus is clearly depicted (black arrows). A small aneurysm (white circle) is also visible with both X-ray and MRA. Temporal footprint = 8 sec.

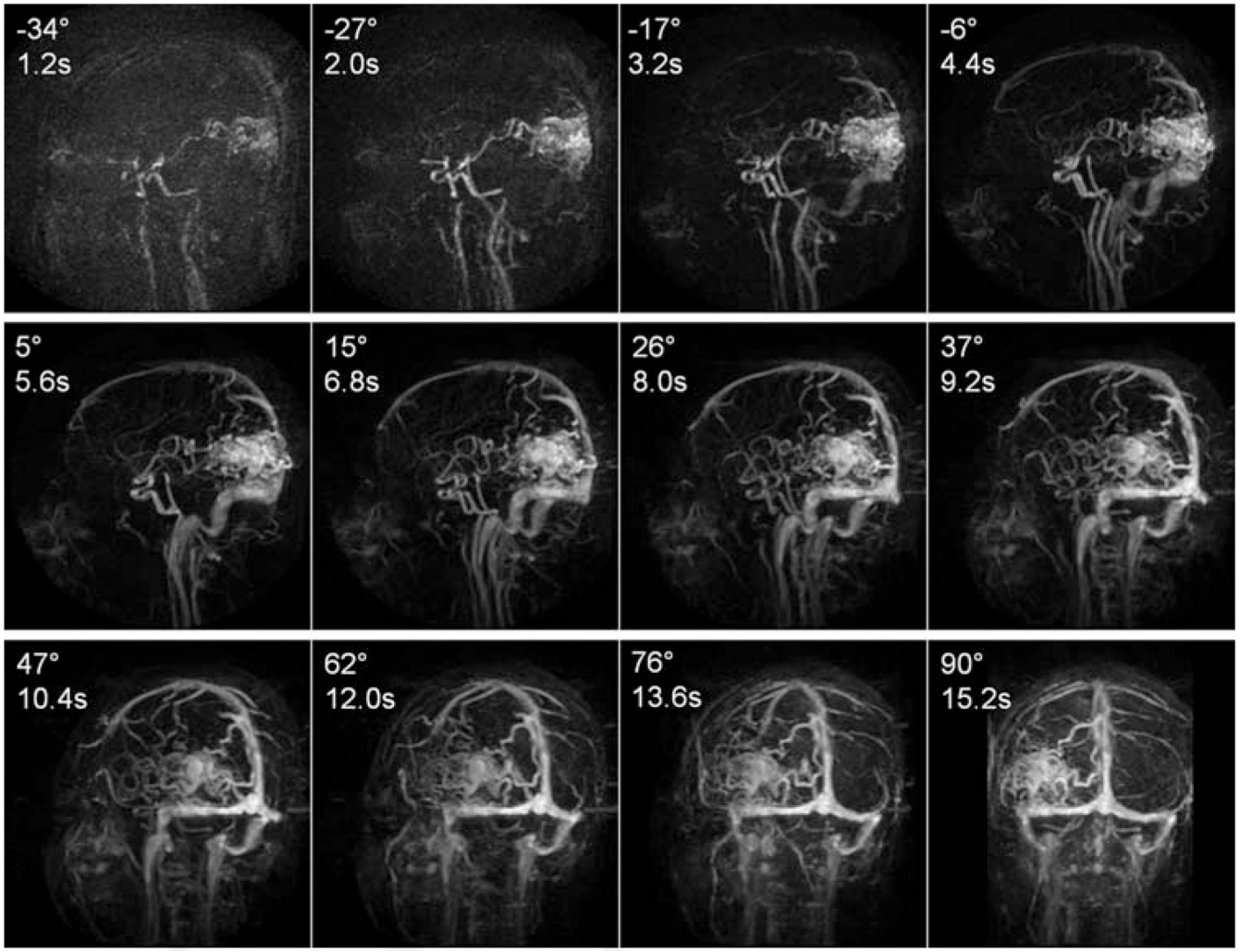

FIG. 9.

Whole-head four-dimensional MRA using E4-GRAPPA. A healthy volunteer was scanned using E4-GRAPPA with a temporal footprint of 6.5 sec. The images show different points in time at different angles relative to the sagittal view.

Table 1

Acceleration Factor, Field of View, Spatial Resolution, Temporal Footprint, and TR for Each CAMERA Protocol

Protocol	Acceleration factor	Field of view (mm^3)	Spatial resolution (mm^3)	Temporal footprint (sec)	TR (ms)
E1	1×	220 × 220 × 96	1.1 × 1.1 × 3	18.4	3
E1-GRAPPA	2×	220 × 220 × 96	1.1 × 1.1 × 3	9.2	3
E4	2×	220 × 220 × 96	1.1 × 1.1 × 3	9.5	6.2
E4-GRAPPA	4×	220 × 220 × 96	1.1 × 1.1 × 3	4.8	6.2
E4-GRAPPA whole head	4×	220 × 220 × 154	1.1 × 1.1 × 3.2	6.3	5.5